ACS APPLIED MATERIALS & INTERFACES

www.acsami.org

Research Article

Organic Anion Detection with Functionalized SERS Substrates via Coupled Electrokinetic Preconcentration, Analyte Capture, and Charge Transfer

Monika Poonia, Timo Küster, and Geoffrey D. Bothun*

Cite This: https://doi.org/10.1021/acsami.2c02934

Read Online

ACCESS | Metrics & More | Article Recommendations

ABSTRACT: Detecting ultralow concentrations of anionic analytes in solution by surface-enhanced Raman spectroscopy (SERS) remains challenging due to their low affinity for SERS substrates. Two strategies were examined to enable *in situ*, liquid phase detection using 5(6)-carboxyfluorescein (5(6)-FAM) as a model analyte: functionalization of a gold nanopillar substrate with cationic cysteamine self-assembled monolayer (CA-SAM) and electrokinetic preconcentration (EP-SERS) with potentials ranging from 0 to +500 mV. The CA-SAM did not enable detection without an applied field, likely due to insufficient accumulation of 5(6)-FAM on the substrate surface limited by passive diffusion. 5(6)-FAM could only be reliably detected with an applied electric field with the charged molecules driven by electroconvection to the substrate surface and the SERS intensity following the Langmuir adsorption model. The obtained limits of detection (LODs) with an applied field were 97.5 and 6.4 nM on bare and CA-SAM substrates, respectively. For the CA-SAM substrates, both the ligand and analyte displayed an ~15-fold signal enhancement with an applied field, revealing an additional enhancement due to charge-transfer resonance taking place between the metal and 5(6)-FAM that improved the LOD by an order of magnitude.

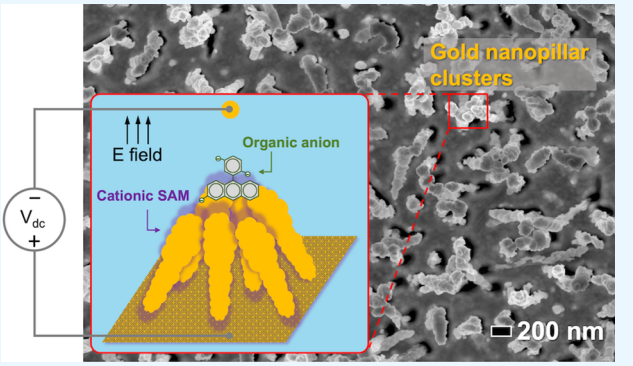

KEYWORDS: *surface-enhanced Raman spectroscopy, electrokinetic preconcentration, charge-transfer resonance, in situ detection, carboxyfluorescein*

INTRODUCTION

Surface-enhanced Raman spectroscopy (SERS) is a powerful detection technique that has attracted a significant amount of attention in various fields including environmental monitoring,[1,2] medicine,[3] forensics science,[4,5] biomedical diagnostics,[6,7] and food safety.[8] SERS measures the frequency-shifted inelastic scattering caused by the vibrational modes of a target analyte molecule relative to the energy of an incident laser[9] and has been reported to achieve label-free molecular fingerprinting at a single-molecule level.[10] The enhancement effect of SERS is attributed to two factors: electromagnetic field enhancement resulting from localized surface plasmon resonance (LSPR) at a nanostructured metal surface[11] and chemical enhancement due to charge transfer between analytes and metal surfaces.[12]

Quantitative SERS analysis is still a challenge for analytes at ultralow concentrations.[13] The SERS effect is localized within the first layer of adsorbed analytes within a few nanometers of a metallic surface. Confining target molecules within SER hot spots produced by LSPR is necessary for sensitive detection.[14] Given that the concentrations of chemical pollutants in environmental matrices are typically in the ng L^{-1} to μg L^{-1} (parts per trillion to parts per billion) range,[15] a preconcentration step is often required. Reported preconcentration strategies for the selective improvement of SERS signal intensities include optofluidic,[16] screen-printed electrodes,[17] dielectrophoresis,[18] optoelectrical trapping,[19] and nanochannel/nanomembrane-based techniques.[20]

Electrokinetic preconcentration (EP) is one mechanism that can be used to draw charged analytes toward SERS substrates through electrostatic forces by applying an electric potential.[21−24] EP-SERS requires that the plasmonic SERS substrates be electrically conducting and stable under the working voltage. For example, gold-decorated pillar-like silicon nanostructures or silver nanoparticle-decorated glass nanopillar arrays have been used as electrodes to enable EP of adenine and rhodamine 6G with a 2−8 order of magnitude improve-

Received: February 16, 2022
Accepted: April 21, 2022

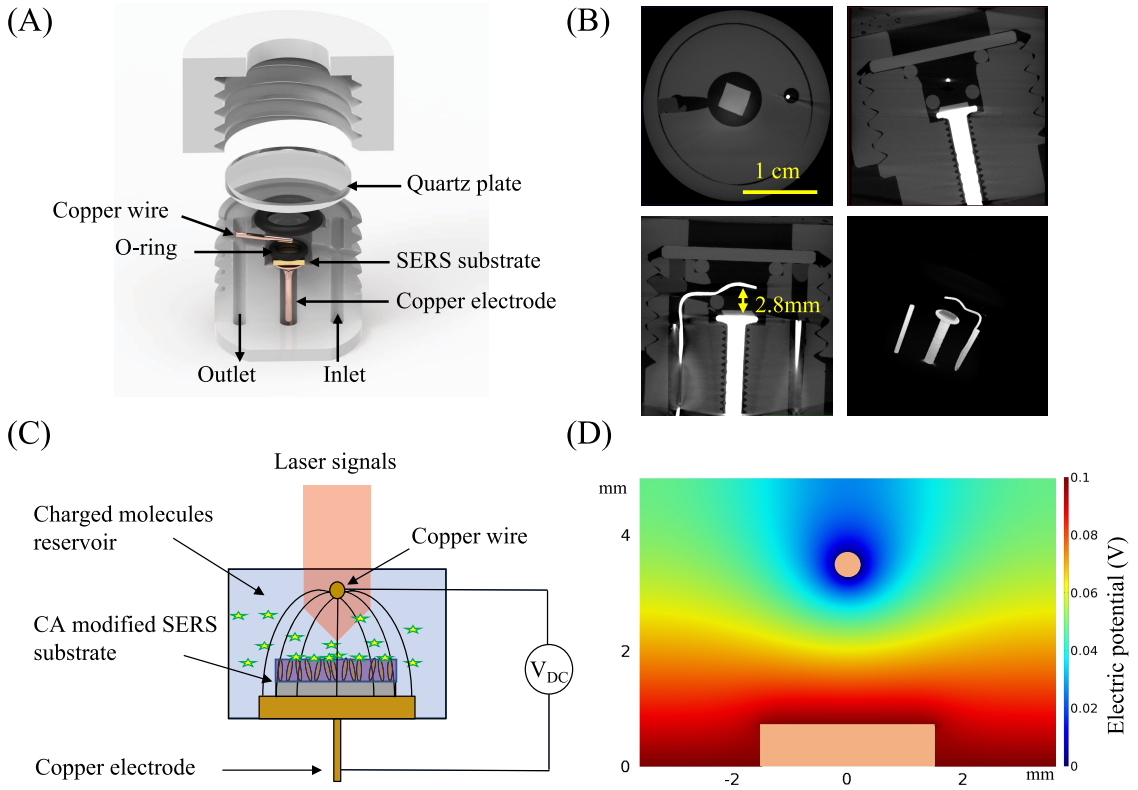

Figure 1. (A) Rendering of the PTFE flow channel device fitted with Cu electrodes for electrokinetic preconcentration. (B) XRM images of an assembled device showing the internal structure at different orientations. (C) Schematic of the EP process and *in situ* SERS measurement. (D) Simulated electric potential distribution around a flat gold substrate at an applied potential of +100 mV.

ment in the detection limit.[25,26] EP-SERS has also been shown to improve the detection of the milk adulterant melamine,[27] drug metabolites,[28] pesticides,[29] uric acid,[30] antibiotics,[31] polar organics,[32] and bacterial screening.[33]

Cysteamine (CA) is a common surface ligand for modifying gold surfaces. CA forms self-assembled monolayers (SAMs) on Au surfaces, and at neutral pH, the primary amine group of CA is protonated and yields a positive surface charge. The amine group also forms strong hydrogen bonds with carboxylic acids. When biomolecules[34] or organic acids[35] are adsorbed via charge attraction and/or H-bonding, CA has been shown to facilitate charge transfer with gold electrodes. Thus far, sensing applications using CA as a charge-transfer agent have been primarily based on standard electrochemical techniques. Those based on SERS have used CA to attract anionic molecules[36] or ions to a substrate surface and have not explicitly considered the role of charge transfer. One drawback of utilizing surface ligands in SERS applications is signal reduction due to chemical interface dampening. However, recent work by Simone and van de Donk[37] suggests that CA may, in fact, enhance SERS due to the electron-withdrawing nature of the terminal $-NH_3^+$ group that promotes metal to ligand charge transfer.

We present a new approach to EP-SERS where an electric field is applied to drive an anionic organic analyte to the substrate surface and a cationic ligand, CA, is used (1) to "capture" the adsorbing analyte and (2) to utilize the charge-transfer behavior of the CA for improved SERS intensity. The goal was to enable *in situ* continuous detections on fully hydrated SERS substrates. A reusable poly(tetrafluoroethylene) (PTFE) flow channel device was designed with a preconcentration chamber between a Cu electrode and a gold nanopillar-array SERS substrate. Low, positive applied potentials were used as CA is reduced on gold surfaces under negative potentials[38] and is oxidized at high positive potentials.[39] The charge-transfer mechanism, taking place between the metal surface and analyte, resulted in significantly higher SERS intensities for the model anionic analyte 5(6)-carboxyfluorescein (5(6)-FAM), allowing for low limits of detection (LODs). Reliable detection was not observed without an applied field for either bare or CA-functionalized substrates. 5(6)-FAM showed the highest surface affinity and strongest SERS signals with applied potential on CA-functionalized surfaces. Without the CA ligand, it would not have been possible to identify this additional enhancement based on the analyte alone. This approach is novel in that an analyte is trapped on CA-modified SERS substrates via electrokinetic preconcentration, where the combination of CA ligands and applied potential facilitate charge transfer, leading to increases in organic ion detection *in situ*.

RESULTS AND DISCUSSION

Device Design. For the proposed EP-SERS, 5(6)-FAM molecules were directed onto the SERS substrates by the application of an external electric field. A custom PTFE semibatch device was fitted with copper (Cu) electrodes; an external electrode was inserted at the top of the internal working volume of the device (165 μL) and a SERS substrate affixed on a copper stage was the working electrode (Figure 1A). Three-dimensional (3D) X-ray microscopy (XRM) images of an assembled device at different orientations show

https://doi.org/10.1021/acsami.2c02934
ACS Appl. Mater. Interfaces XXXX, XXX, XXX−XXX

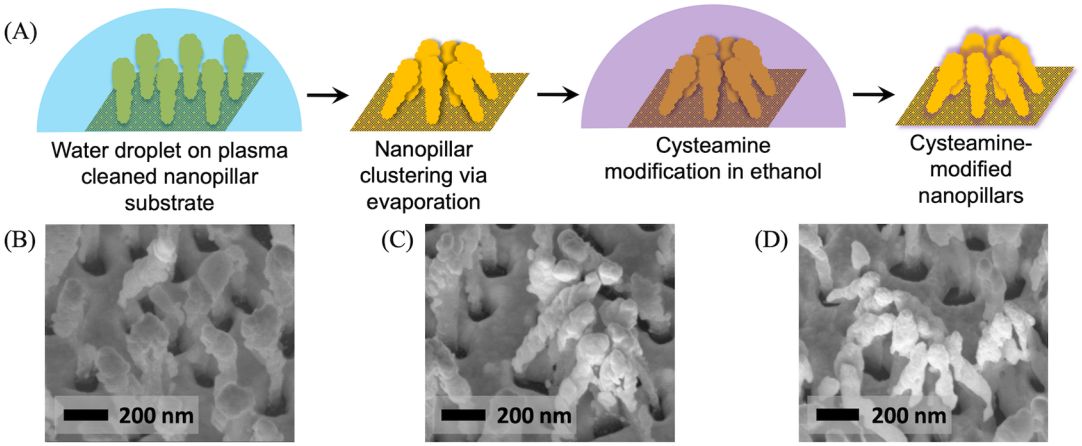

Figure 2. (A) Cysteamine (CA) surface modification of SERS substrates with gold-coated silicon nanopillars. FE-SEM images show (B) as-received and preleaned nanopillars (C) without and (D) with CA during the modification process.

the internal structure and details of the chamber (Figure 1B) with the SERS substrate visible between the electrodes. The mean gap between electrodes, d, was 2.8 mm. A schematic of the EP process on a SERS substrate is shown in Figure 1C. There was no measurable current at the level of 1 mA between the electrodes over the range of electric potentials examined. An example of the electric potential distribution within the device derived from COMSOL simulations is shown in Figure 1D at an applied voltage of +100 mV, indicating that the potential was uniform across the surface of the SERS substrate. SERS measurements were conducted in semibatch mode with no stirring, relying on the passive diffusion or electroconvection of the analyte in the absence or presence of an electric field, respectively.

SERS Substrates and Cysteamine Functionalization. SERS substrates with freestanding nanopillars coated with gold act as effective SERS substrates by trapping analytes near the electromagnetic hot spots.[40] Hot spots are formed between nanopillars that lean together due to capillary forces generated by an evaporating analyte solution. Analyte molecules are then "trapped" within the formed hot spots.[41−43] Allowing a droplet of analyte solution to evaporate and lean the nanopillars is the predominant method of analyte detection for such substrates via SERS under dry conditions. In our work on *in situ* analyte detection using EP, the nanopillars were preleaned using deionized water. The high surface tension of water led to many clusters of leaned nanopillars observed by a field emission scanning electron microscope (FE-SEM); 96% of the nanopillars were leaned and formed clusters based on an image analysis of 250 individual nanopillars (results not shown).

SERS measurements of anionic species are limited by low adsorption affinity to metal surfaces, corresponding to low accumulation within the SERS hot spots. Molecules containing carboxylic acid groups such as 5(6)-FAM can adsorb on SERS substrates but with much weaker affinity than sulfur or nitrogen-containing molecules.[44] Substrates with preleaned nanopillars were functionalized with positively charged CA to increase the affinity of anionic species with the surface (Figure 2). CA spontaneously forms self-assembled monolayers (SAMs) on gold surfaces, is stable in water, and promotes a hydrophilic environment.[36,45] CA-SAMs have been shown to achieve approximately 80% surface coverage on gold surfaces within 5 min of exposure to ethanolic solutions with millimolar CA concentrations.[39] SERS spectra of a nonmodified substrate and a substrate modified with CA confirmed the presence of a CA-SAM (Figure 3A). Two strong characteristic CA peaks were observed between 600 and 800 cm^{-1} due to C−S stretching vibrations. The band at 644 cm^{-1} is attributed to the C−S stretching vibration for a gauche (G) conformation and the band at 724 cm^{-1} is attributed to the trans (T) conformation (Figure 3A inset).[46] The ratio of these two bands is indicative of the relative concentration of each conformer, which has been shown to shift from T to G over time as CA molecules desorb from the initial T conformation and readsorb in the G conformation. The measured G/T ratio was ∼0.5 and, as discussed below, there was no apparent change in this ratio over the durations examined in this work in the absence of the model analyte 5(6)-FAM or without an applied electric potential.

SERS was conducted under 0 and +100 mV potentials as a function of time to investigate the effect of an applied electric field on the CA-SAMs without an analyte present. The peak intensities of CA at 644 cm^{-1} (G) and 724 cm^{-1} (T) are shown in Figure 3B,C, respectively. The intensity of the G and T peaks increased 4.8- and 5.6-fold, respectively, 5 min after applying the field. Fluctuations in the intensity of the T conformer (Figure 3C) indicate changes in molecular orientation relative to the surface, whereas the intensity of the G peak was stable and increased over the first 20 min of the applied field before plateauing. In the G conformation, the molecules lay flat on the surface and maximize their attractive interactions with the SERS substrate.

We assert that the most plausible explanation for SERS enhancement induced by the applied potential is charge-transfer (CT) resonance between Au and CA. By mapping the electron density of CA-capped Au nanofilms used as a SPR sensor, Simone and van de Donk[37] have shown that electrons in Au are transferred to CA due to attraction with the terminal $-NH_3^+$ group and suggest that charge is localized near the Au−S bond. Mechanistically, this involves electron transfer from the highest occupied molecular orbitals (HOMO) of Au, also referred to as the Fermi energy (E_F) or work function, to the lowest unoccupied molecular orbital (LUMO) of CA (S orbitals). The E_F-LUMO energy gap is further reduced to promote CT through surface functionalization, which is known to reduce E_F in metals by altering electric dipole moments at the Au surface, and by manipulating E_F with an applied potential, which has been shown to improve SERS detection of

https://doi.org/10.1021/acsami.2c02934
ACS Appl. Mater. Interfaces XXXX, XXX, XXX−XXX

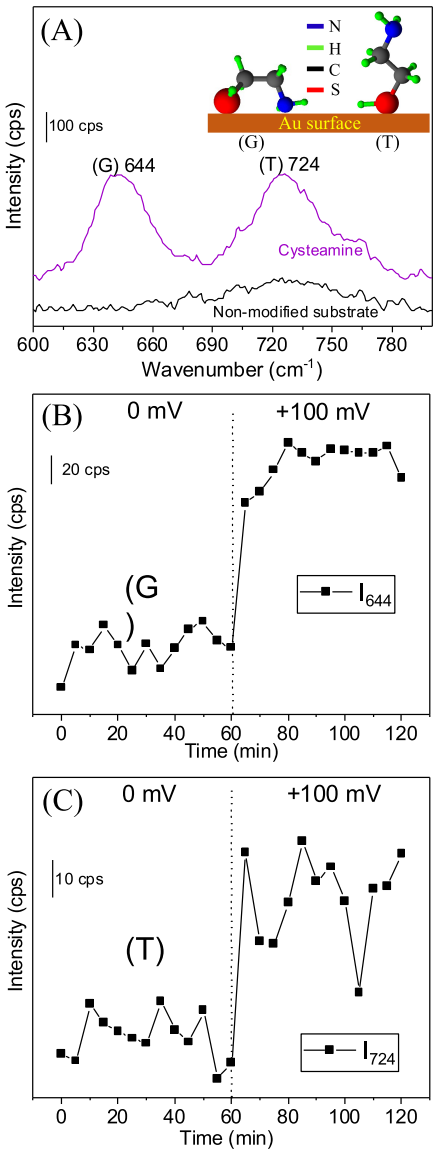

Figure 3. (A) SERS spectra recorded from a nonmodified substrate (black) and from a preleaned substrate modified with CA (purple) with an integration time of 10 s. The inset shows the likely structures of adsorbed CA molecules in the trans (T) or gauche (G) conformation. SERS intensity vs time is shown for the (B) G and (C) T peaks at applied potentials of 0 and +100 mV.

aromatic thiols such as 4-aminobenzene thiol (4-ABT) on Au.[47]

Electrokinetic Preconcentration of 5(6)-FAM. 5(6)-FAM was chosen as a probe molecule due to its strong Raman activity.[48−51] Organic dyes are commonly used in textile and dyeing industries, and wastewater from these industries adversely affects aquatic ecosystems.[52] Thus, organic dye detection is extremely important in environmental monitoring. As dye molecules such as 5(6)-FAM approach a metal surface, the close proximity to the surface provides a nonradiative pathway for relaxation from an excited state, which quenches the fluorescence for SERS applications.[53,54]

For proof-of-concept and to identify a suitable range of applied potentials, SERS was conducted with 1 μM 5(6)-FAM using CA-SAM substrates and peak intensities were recorded over time with potentials ranging from +100 to +500 mV corresponding to electric field strengths ($E = V(dK)^{-1}$ where $K = \varepsilon\varepsilon_0$ is the dielectric constant for water) of approximately 36−179 V m^{-1}. At these field strengths, the calculated limiting velocity (v) range for 5(6)-FAM is 0.6−3.1 μm s^{-1} based on Stokes Law, $v = zeE(6\pi\eta r)^{-1}$, where z is the number of charges (1 at pH 7), e is the elemental electron charge, η is viscosity (1 mPa·s for water at 20 °C), and r is the Stokes radius (0.49 nm) based on the estimated diffusion coefficient, D, for 5-FAM (4.2 × 10^{-10} m^2 s^{-1}).[55] Setting the characteristic length, L, equal to the mean gap between the electrodes, the Peclet number ($Pe_L = LvD^{-1}$) ranged from 4.2 to 20.7. A $Pe_L > 1$ indicates that convective transport of 5(6)-FAM within the electric field exceeded diffusion, which is necessary to achieve electrokinetic preconcentration.

Two prominent peaks of 5(6)-FAM for phenolic (C−OH) bend at 1177 cm^{-1} (Figure 4A) and C−C stretching within the xanthene ring at 1330 cm^{-1} (Figure 4B) were monitored. 5(6)-FAM signals were low at 0 mV and were amplified 6-fold upon applying a potential of +100 mV. Full spectra are shown in Figure 4C with additional peaks for in-plane ring vibration at 1503 cm^{-1} and C−O and/or C−C stretching within the xanthene ring at 1636 cm^{-1}. The Raman bands at 1177 and 1330 cm^{-1} increased linearly over 60 min at +100 mV (Figure 4A−D). Increasing the applied potential led to additional preconcentration up to +300 mV (Figure 4A,B). Decreases in the intensities at higher potentials, +400 and +500 mV, are attributed to the oxidation of CA. CA oxidation on a gold electrode has been shown to begin at approximately +400 mV due to the oxidation of the SH group of the thiols, which then leads to CA desorption.[39] To prevent CA oxidation and given that the primary preconcentration step occurs at +100 mV, this potential was selected for further studies over a range of 5(6)-FAM concentrations from 1 nM to 10 μM.

SERS spectra were recorded under four conditions: nonmodified and CA functionalized with and without an applied potential (Figure 5). Adsorption isotherms were generated based on the peak intensity at 1330 cm^{-1} according to the Langmuir adsorption model, assuming that the SERS intensity, I, was directly proportional to the concentration of 5(6)-FAM bound to the surface. I is the measured intensity after a substrate was exposed to each 5(6)-FAM concentration for 30 min.

$$I = \frac{I_{sat}K[5(6)-\text{FAM}]}{1 + K[5(6)-\text{FAM}]} \quad (1)$$

In eq (1), I_{sat} is the saturated intensity, [5(6)-FAM] is the bulk concentration, and K is the Langmuir constant defined as

$$K = \frac{[S_{Au}5(6)-\text{FAM}]}{[S_{Au}][5(6)-\text{FAM}]} \quad (2)$$

where $[S_{Au}]$ is the concentration of free surface binding sites and $[S_{Au}5(6)\text{-FAM}]$ is the concentration of sites with bound 5(6)-FAM.

The 5(6)-FAM signal was low and did not correlate with 5(6)-FAM concentration for the nonmodified substrate without an applied field, implying low surface adsorption (Figure 5A). With an applied field, the nonmodified substrate exhibited Langmuir adsorption behavior with a K = 0.013 nM^{-1} and R^2 = 0.72, indicating a good fit of the model and demonstrating EP (Figure 5B). Results for CA functionalization alone, without an applied field, were similar to results for the nonmodified substrate and showed that the cationic CA-

https://doi.org/10.1021/acsami.2c02934
ACS Appl. Mater. Interfaces XXXX, XXX, XXX−XXX

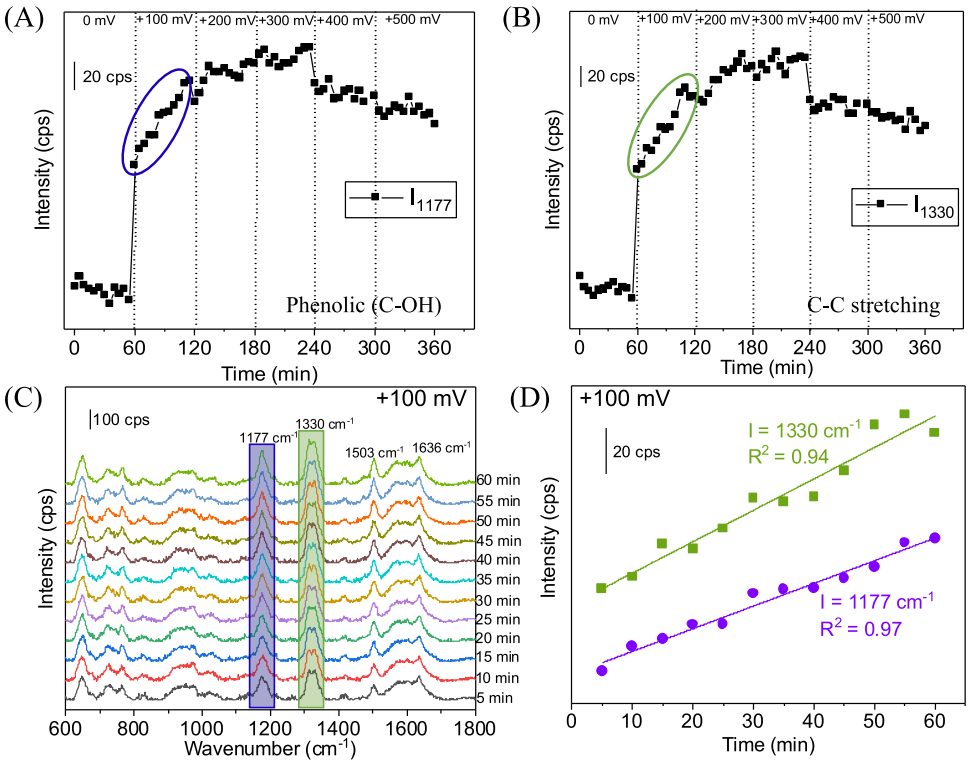

Figure 4. SERS intensities measured *in situ* as a function of time for 5(6)-FAM peaks on CA-SAM-modified substrates at (A) 1177 and (B) 1330 cm^{-1} with applied potentials ranging from 0 to +500 mV. (C) SERS spectra of 5(6)-FAM at +100 mV applied potential for 60 min with the integration time of 10 s. (D) SERS intensity and the preconcentration time associated with 5(6)-FAM peaks at 1177 and 1330 cm^{-1} at +100 mV. In all cases, the 5(6)-FAM concentration was 1 μM.

SAMs did not lead to sufficient accumulation of anionic 5(6)-FAM within the SERS hot spots over the timeframe examined (Figure 5C). The most sensitive 5(6)-FAM detection was achieved by combining CA-SAMs with an applied field (Figure 4D). An excellent fit to the Langmuir adsorption model was obtained, $R^2 = 0.97$, yielding $K = 0.029\ nM^{-1}$, which represents a 2.2-fold increase in the Langmuir constant with CA functionalization compared to the nonmodified substrate.

Experimental enhancement factors (EFs) are commonly used to describe improved analyte detection via SERS. EFs for 5(6)-FAM on bare and CA-SAM-modified substrate in the presence of applied potential were determined as[56]

$$EF = \frac{I_{SERS} \times C_{Raman}}{I_{Raman} \times C_{SERS}} \quad (3)$$

where I_{SERS} is the intensity of 5(6)-FAM at 1180 cm^{-1} for bare and CA-SAM-modified substrates in the presence of the electric field, I_{Raman} is the intensity of the 5(6)-FAM solution at 1180 cm^{-1}, C_{SERS} is the concentration of 5(6)-FAM for bare (100 nM) and CA-SAM modified (10 nM) substrates, and C_{Raman} is the solution concentration of 5(6)-FAM (100 μM). EFs were approximately 1×10^4 and 6×10^4 for bare and CA-modified substrates, respectively. The 6-fold increase in EF is attributed to 5(6)-FAM capture by the oppositely charged CA-SAM during electrokinetic preconcentration.

Limits of detection (LODs) were calculated to further demonstrate the synergistic effects of CA-SAMs and an applied field according to the equation

$$I_b = \underline{I_b} + 3 \cdot \sigma_b \quad (4)$$

where I_b is the intensity at the LOD, $\underline{I_b}$ is the mean intensity obtained from the spectra, and σ_b is the standard deviation of a blank spectrum. The LOD concentration can be calculated by substituting I_b for I in eq (1) and solving for [5(6)-FAM].[1,57,58] A 15-fold improvement in the LOD was observed for the CA-functionalized substrate (6.4 nM) compared to the nonmodified substrate (97.5 nM). These quantitative results suggest that EP-SERS with CA-SAMs can be applied to detect and monitor charged organic anions in a solution with high sensitivity.

As shown in the literature,[45] in the absence of an electric field, one might expect an increase in the 5(6)-FAM intensity due to attractive interactions between CA-SAMs and 5(6)-FAM, such as electrostatic, cation-π, or hydrogen bonding. However, our results indicate that only the application of an electric field with a CA-SAM present led to noticeable signal enhancement. The mechanism of 5(6)-FAM signal enhancement can be inferred based on the Langmuir adsorption results with and without CA-SAM functionalization (Figure 6). The enhancement with an applied field is due to the charge transfer between the metal and CA. In the absence of a CA-SAM, 5(6)-FAM is drawn to the surface via electroconvection and signal enhancement is attributed to CT. On CA-SAM-modified substrates, signal enhancement of CA, as well as adsorbed 5(6)-FAM, is observed consistent with CT for both the capture ligand and the target analyte. This important discovery suggests that CA does not cause chemical interference with the analyte of interest, 5(6)-FAM, but rather enhances its signal by trapping it on the surface and facilitating CT.

https://doi.org/10.1021/acsami.2c02934
ACS Appl. Mater. Interfaces XXXX, XXX, XXX−XXX

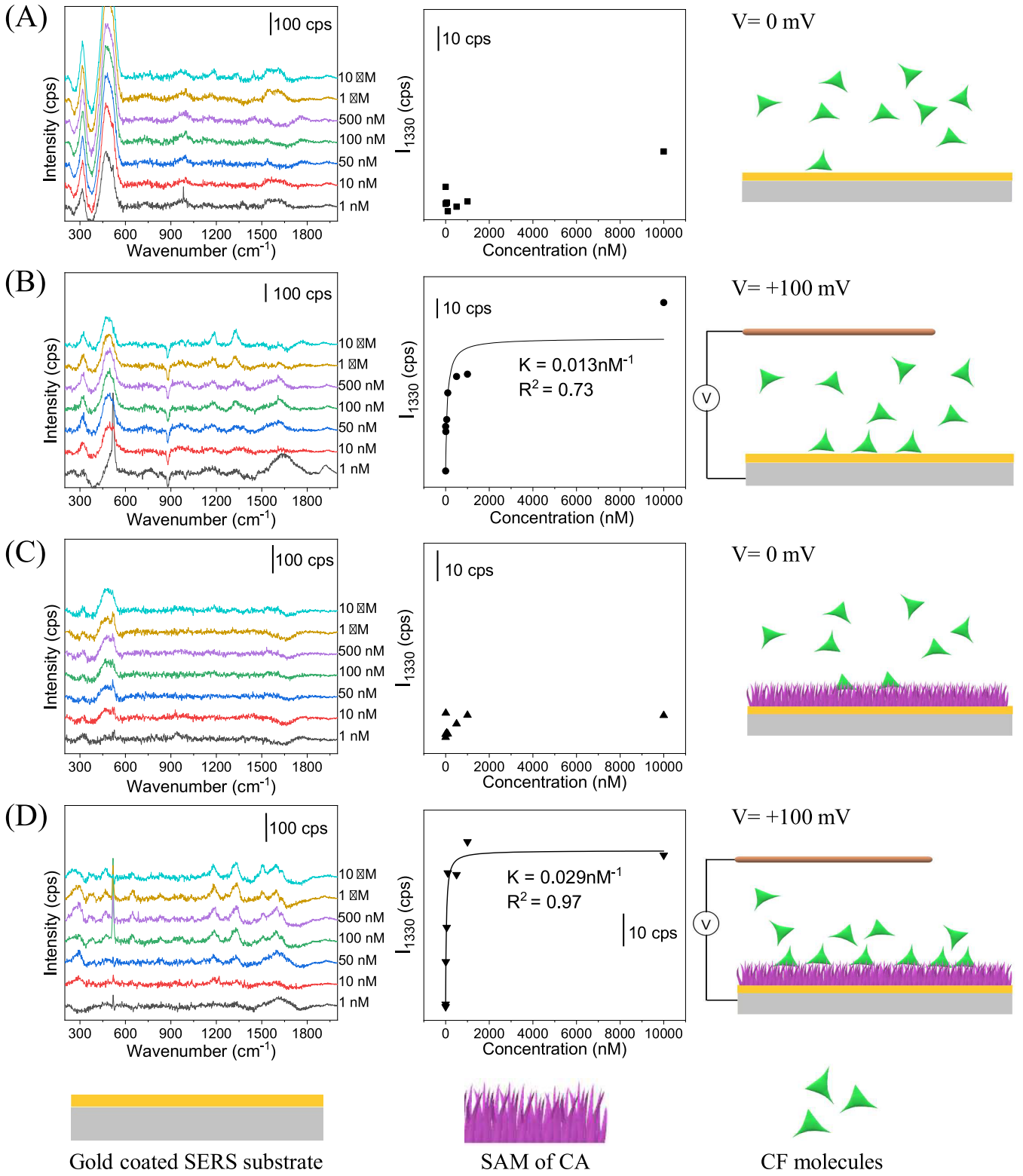

Figure 5. SERS spectra (left) as a function of 5(6)-FAM concentration with nonmodified substrates at (A) 0 mV and (B) +100 mV and with CA-functionalized substrates at (C) 0 mV and (D) +100 mV. Spectra are shown after background subtraction. The SERS intensities at 1330 cm^{-1} are shown (center) as a function of 5(6)-FAM concentration. The solid lines represent the fitted Langmuir adsorption model. Schematic representations are shown (right) depicting EP (not to scale).

CONCLUSIONS

Electrokinetic preconcentration and synergistic effects with combined cysteamine surface functionalization led to the sensitive detection of a model anionic analyte, 5(6)-FAM, in water on fully hydrated nanopillar SERS surfaces. This was achieved by selecting an applied potential below the oxidation threshold for cysteamine and modeling the signal response curve using the Langmuir adsorption model. The SERS enhancement is attributed to a combination of charge-transfer

https://doi.org/10.1021/acsami.2c02934
ACS Appl. Mater. Interfaces XXXX, XXX, XXX−XXX

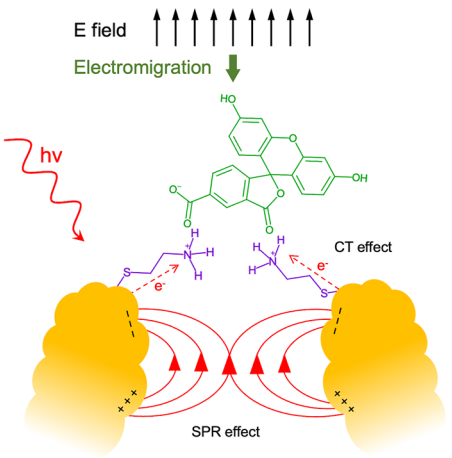

Figure 6. Schematic illustration of 5(6)-FAM (green) capture and detection on the nanopillar SERS substrates modified with CA (purple) (not to scale). Excitation energy, *hν*, and the SPR and CT effects contributing to SERS enhancement are shown (red arrows) along with the direction of the electric field and the electromigration of 5(6)-FAM.

resonance, electrokinetic phenomena, and intermolecular interactions between anionic carboxyfluorescein and cationic cysteamine. This work opens a potential new pathway toward *in situ*, high-sensitivity SERS for rapid detection of dissolved organic ions. Additional studies on the effects of, for example, electrolytes and interfering species can be used to design substrates and processes for industrial and field applications ranging from environmental monitoring to food safety and chemical manufacturing.

METHODS

Materials. 5(6)−Carboxyfluorescein (5(6)-FAM, HPLC-grade, ≥95%) and cysteamine (CA, ∼95%) were purchased from Sigma-Aldrich. Aqueous 5(6)-FAM solutions were prepared with ultrapure MilliQ water (resistivity >18.2 MΩ-cm at 25 °C). Ethanol was purchased from Fisher Scientific (Histological grade). All materials were used as received, and solutions were stored in the dark at 4 °C. Molecular property predictions were made using MarvinSketch (Chemaxon).

SERS Substrates. "SERStrate" SERS substrates with gold-capped silicon nanopillars were purchased from Silmeco ApS (Copenhagen, Denmark). Schmidt et al.[40] provide a complete description of the fabrication, enhancement mechanism, and intrinsic properties of the substrates. Nanopillars were leaned together to form hot spots before surface functionalization by depositing a droplet of water on the substrates and drying under ambient conditions for 30 min. Field enhancement takes place in the space between the leaned nanopillars.[59] Substrates were treated with an oxygen-plasma cleaner (Diener electronic, Germany) for 5 min at 30 W and 0.2 Torr to remove surface contamination and improve substrate wetting before functionalization. Plasma cleaning reduced the background signal and yielded higher analyte signal intensities.[60] Electron microscopy images of SERS substrates before and after leaning the nanopillars were obtained with a Zeiss Sigma VP field emission scanning electron microscope (FE-SEM) using an Everhart−Thornley secondary electron detector at an accelerating voltage of 7 kV.

For surface functionalization, a self-assembled monolayer (SAM) was formed on plasma cleaned and preleaned SERS substrates. The SAM was formed using a solution of 10 mM CA in ethanol and submerged the SERS substrates in 1 mL of this solution for 24 h. Substrates were thoroughly rinsed with ethanol and dried under ambient conditions for 30 min.

SERS Equipment. SERS spectra were collected using a SIERRA 2.0 Raman spectrometer (Snowy Range Instruments, WY, USA) equipped with a 785 nm laser. Measurements were conducted with a 100 mW laser with a spot diameter of ∼40 μm over integration times ranging from 1 to 20 s. Orbital Raster Scanning (ORS) was used for all measurements providing an effective SERS detection area 2 mm in diameter. ORS provided a $\sim 10^3$ increase in the detection area, increasing the number of accessible surface hot spots and reducing measurement variability across multiple SERS substrates. All of the spectra were collected in the wavenumber range 200−2000 cm^{-1} with a spectral resolution of 4 cm^{-1}.

Device Fabrication and Configuration. A poly(tetrafluoroethylene) (PTFE) flow channel (Figure 1A) was designed for the electrochemical SERS measurements. The channel consists of an inlet, an outlet, two electrode ports at the top and the bottom, and a quartz window for Raman measurements. Two copper electrodes were used with a separation distance of ∼2.8 mm, and the internal working volume of the preconcentration chamber was 165 μL. A Cu nail was used as the bottom electrode, also serving as a conductive base to affix the SERS substrates, and a Cu wire was used as the counter electrode. A rubber O-ring was used to hold the substrate in position. A poly(lactic acid) holder was designed for positioning the flow device under the Raman spectrometer via 3D printing with a MakerBot Replicator+.

3D X-ray microscopy was used to visualize the internal structure and details of the in-house built PTFE flow channel. The tomography was run on a Zeiss Xradia Versa 610 running at 160 kV and 25 W, with a full 360° acquisition and 3001 projections, 2 s integration time, and a voxel size of 25 μm. In XRM, regions of the specimen composed of atoms with high atomic weight (steel, copper) appear white, while regions of the specimen with air appear black. Regions with intermediate atomic weight (polymer, silicon) appear as different shades of gray.

***In Situ* Electrochemical SERS Measurement.** A 3 mL syringe (BD, Luer-Lok tip) connected to chemically resistant tubing was used to fill the chamber with the sample solution. Fresh 5(6)-FAM solution with concentrations from 1 nM to 10 μM were introduced into the chamber through the inlet, and measurements were conducted under applied electric potentials ranging from 0 to +500 mV using a commercial DC power supply source (KORAD, KA3005D). While switching to higher concentrations of 5(6)-FAM, the chamber was cleaned by flushing it with 9 mL of ultrapure water, equivalent to 55 times the working volume of the preconcentration chamber.

The SERS spectra were baselined using the Bayesian method, implemented in the "CrystalSleuth" software (Version 2008, (RRUFF, AZ)).[61] To remove the background, the control spectrum was subtracted from all other concentrations of 5(6)-FAM and background subtracted spectra were analyzed with OriginPro (Version 2019b, OriginLab Corp., Northampton MA).

Simulations. A commercially available finite element method (FEM) simulation software (COMSOL Multiphysics, 4.2) was used to determine the local electric field generated in the preconcentration chamber under an applied potential of +100 mV (Figure 1D). The size of the substrate was set to 3 × 3 mm, and the depth of the chamber was set to 4 mm in the simulation. The gap between the substrate and top electrode was set to 2.8 mm.

AUTHOR INFORMATION

Corresponding Author

Geoffrey D. Bothun − *Department of Chemical Engineering, University of Rhode Island, Kingston, Rhode Island 02881, United States;* orcid.org/0000-0002-7513-2417; Phone: +1-401-874-9518; Email: gbothun@uri.edu

Authors

Monika Poonia − *Department of Chemical Engineering, University of Rhode Island, Kingston, Rhode Island 02881, United States;* orcid.org/0000-0002-8531-1603

https://doi.org/10.1021/acsami.2c02934
ACS Appl. Mater. Interfaces XXXX, XXX, XXX−XXX

Timo Küster − *Department of Chemical Engineering, University of Rhode Island, Kingston, Rhode Island 02881, United States*

Complete contact information is available at: https://pubs.acs.org/10.1021/acsami.2c02934

Notes

The authors declare no competing financial interest.

■ ACKNOWLEDGMENTS

This material is based upon work supported in part by the National Science Foundation under EPSCoR Cooperative Agreements #OIA-1655221 and #OIA-1004057. Any opinions, findings, and conclusions or recommendations expressed in this material are those of the author(s) and do not necessarily reflect the views of the National Science Foundation. The FE-SEM and 3D-XRM data were acquired at the RI Consortium for Nanoscience and Nanotechnology, a URI College of Engineering core facility partially funded by the National Science Foundation EPSCoR, Cooperative Agreement #OIA-1655221, and the RI 401 Tech Bridge Innovation Campus. The authors would like to thank Dr. Irene Andreu for her support with microscopy.

■ REFERENCES

(1) Küster, T.; Bothun, G. D. In situ SERS Detection of Dissolved Nitrate on Hydrated Gold Substrates. *Nanoscale Adv.* **2021**, *3*, 4098−4105.

(2) Lv, L.; He, L.; Jiang, S.; Chen, J.; Zhou, C.; Qu, J.; Lu, Y.; Hong, P.; Sun, S.; Li, C. In situ Surface-Enhanced Raman Spectroscopy for Detecting Microplastics and Nanoplastics in Aquatic Environments. *Sci. Total Environ.* **2020**, *728*, No. 138449.

(3) Xie, W.; Schlücker, S. Medical Applications of Surface-Enhanced Raman Scattering. *Phys. Chem. Chem. Phys.* **2013**, *15*, 5329−5344.

(4) Fikiet, M. A.; Khandasammy, S. R.; Mistek, E.; Ahmed, Y.; Halámková, L.; Bueno, J.; Lednev, I. K. Surface Enhanced Raman Spectroscopy: A review of Recent Applications in Forensic Science. *Spectrochim. Acta, Part A* **2018**, *197*, 255−260.

(5) Muehlethaler, C.; Leona, M.; Lombardi, J. R. Review of Surface Enhanced Raman Scattering Applications in Forensic Science. *Anal. Chem.* **2016**, *88*, 152−169.

(6) Huang, Z.; Zhang, A.; Zhang, Q.; Cui, D. Nanomaterial-Based SERS Sensing Technology for Biomedical Application. *J. Mater. Chem. B* **2019**, *7*, 3755−3774.

(7) Moisoiu, V.; Stefancu, A.; Gulei, D.; Boitor, R.; Magdo, L.; Raduly, L.; Pasca, S.; Kubelac, P.; Mehterov, N.; Chiş, V.; Simon, M.; Muresan, M.; Irimie, A. I.; Baciut, M.; Stiufiuc, R.; Pavel, I. E.; Achimas-Cadariu, P.; Ionescu, C.; Lazar, V.; Sarafian, V.; Notingher, I.; Leopold, N.; Berindan-Neagoe, I. SERS-based Differential Diagnosis between Multiple Solid Malignancies: Breast, Colorectal, Lung, Ovarian and Oral Cancer. *Int. J. Nanomed.* **2019**, *14*, 6165−6178.

(8) Xie, X.; Pu, H.; Sun, D. Recent Advances in Nanofabrication Techniques for SERS Substrates and their Applications in Food Safety Analysis. *Crit. Rev. Food Sci. Nutr.* **2018**, *58*, 2800−2813.

(9) Mosier-Boss, P. A. Review of SERS Substrates for Chemical Sensing. *Nanomaterials* **2017**, *7*, 142.

(10) Wu, H.-Y.; Choi, C. J.; Cunningham, B. T. Plasmonic Nanogap-Enhanced Raman Scattering Using a Resonant Nanodome Array. *Small* **2012**, *8*, 2878−2885.

(11) Lis, D.; Cecchet, F. Localized Surface Plasmon Resonances in Nanostructures to Enhance Nonlinear Vibrational Spectroscopies: Towards an Astonishing Molecular Sensitivity. *Beilstein J. Nanotechnol.* **2014**, *5*, 2275−2292.

(12) Trivedi, D. J.; Barrow, B.; Schatz, G. C. Understanding the Chemical Contribution to the Enhancement Mechanism in SERS: Connection with Hammett Parameters. *J. Chem. Phys.* **2020**, *153*, No. 124706.

(13) Pérez-Jiménez, A. I.; Lyu, D.; Lu, Z.; Liu, G.; Ren, B. Surface-Enhanced Raman Spectroscopy: Benefits, Trade-offs and Future Developments. *Chem. Sci.* **2020**, *11*, 4563−4577.

(14) Bell, S. E. J.; Charron, G.; Cortés, E.; Kneipp, J.; Chapelle, M. L.; Langer, J.; Procházka, M.; Tran, V.; Schlücker, S. Towards Reliable and Quantitative Surface-Enhanced Raman Scattering (SERS): From Key Parameters to Good Analytical Practice. *Angew. Chem., Int. Ed.* **2020**, *59*, 5454−5462.

(15) Neale, P. A.; Brack, W.; Aït-Aïssa, S.; Busch, W.; Hollender, J.; Krauss, M.; Maillot-Maréchal, E.; Munz, N. A.; Schlichting, R.; Schulze, T.; Vogler, B.; Escher, B. I. Solid-phase Extraction as Sample Preparation of Water Samples for Cell-based and Other in Vitro Bioassays. *Environ. Sci.: Processes Impacts* **2018**, *20*, 493−504.

(16) Choi, J.; Lee, J.; Jung, J. H. Fully Integrated Optofluidic SERS Platform for Real-time and Continuous Characterization of Airborne Microorganisms. *Biosens. Bioelectron.* **2020**, *169*, No. 112611.

(17) Ibáñez, D.; González-García, M. B.; Hernández-Santos, D.; Fanjul-Bolado, P. Detection of Dithiocarbamate, Chloronicotinyl and Organophosphate Pesticides by Electrochemical Activation of SERS Features of Screen-printed Electrodes. *Spectrochim. Acta, Part A* **2021**, *248*, No. 119174.

(18) Lin, H.-Y.; Huang, C.; Hsieh, W.; Liu, L.; Lin, Y.; Chu, C.; Wang, S.; Kuo, I. T.; Chau, L.; Yang, C. On-line SERS Detection of Single Bacterium using Novel SERS Nanoprobes and a Microfluidic Dielectrophoresis Device. *Small* **2014**, *10*, 4700−4710.

(19) Yuan, Y.; Lin, Y.; Gu, B.; Panwar, N.; Tjin, S. C.; Song, J.; Qu, J.; Yong, K. Optical Trapping-assisted SERS Platform for Chemical and Biosensing Applications: Design Perspectives. *Coord. Chem. Rev.* **2017**, *339*, 138−152.

(20) Lee, J. H.; Song, Y.; Han, J. Multiplexed Proteomic Sample Preconcentration Device using Surface-patterned Ion-selective Membrane. *Lab Chip* **2008**, *8*, 596−601.

(21) Yang, Y.; Li, Y.; Zhai, W.; Li, X.; Li, D.; Lin, H.; Han, S. Electrokinetic Preseparation and Molecularly Imprinted Trapping for Highly Selective SERS Detection of Charged Phthalate Plasticizers. *Anal. Chem.* **2021**, *93*, 946−955.

(22) Yan, Z.; Xia, M.; Wang, P.; Zhang, P.; Liang, O.; Xie, Y. Selective Manipulation of Molecules by Electrostatic Force and Detection of Single Molecules in Aqueous Solution. *J. Phys. Chem. C* **2016**, *120*, 12765−12772.

(23) Li, Y.-T.; Qu, L.; Li, D.; Song, Q.; Fathi, F.; Long, Y. Rapid and Sensitive in-situ Detection of Polar Antibiotics in Water using a Disposable Ag−graphene Sensor based on Electrophoretic Preconcentration and Surface Enhanced Raman Spectroscopy. *Biosens. Bioelectron.* **2013**, *43*, 94−100.

(24) Lacharmoise, P. D.; Le Ru, E. C.; Etchegoin, P. G. Guiding Molecules with Electrostatic Forces in Surface Enhanced Raman Spectroscopy. *ACS Nano* **2009**, *3*, 66−72.

(25) Park, M.; Oh, Y.; Park, S.; Yang, S.; Jeong, K. Electrokinetic Preconcentration of Small Molecules Within Volumetric Electromagnetic Hotspots in Surface Enhanced Raman Scattering. *Small* **2015**, *11*, 2487−2492.

(26) Cho, H.; Lee, B.; Liu, G. L.; Agarwal, A.; Lee, L. P. Label-Free and Highly Sensitive Biomolecular Detection Using SERS and Electrokinetic Preconcentration. *Lab Chip* **2009**, *9*, 3360−3363.

(27) Viehrig, M.; Rajendran, S. T.; Sanger, K.; Schmidt, M. S.; Alstrøm, T. S.; Rindzevicius, T.; Zór, K.; Boisen, A. Quantitative SERS Assay on a Single Chip Enabled by Electrochemically Assisted Regeneration: A Method for Detection of Melamine in Milk. *Anal. Chem.* **2020**, *92*, 4317.

(28) Greene, B. H. C.; Alhatab, D. S.; Pye, C. C.; Brosseau, C. L. Electrochemical-Surface Enhanced Raman Spectroscopic (EC-SERS) Study of 6-Thiouric Acid: A Metabolite of the Chemotherapy Drug Azathioprine. *J. Phys. Chem. C* **2017**, *121*, 8084−8090.

(29) Li, D.; Duan, H.; Wang, Y.; Zhang, Q.; Cao, H.; Deng, W.; Li, D. On-Site Preconcentration of Pesticide Residues in a Drop of Seawater by using Electrokinetic Trapping, and their Determination

by Surface-Enhanced Raman Scattering. *Microchim. Acta* **2017**, *185*, No. 10.
(30) Zhao, L.; Blackburn, J.; Brosseau, C. L. Quantitative Detection of Uric Acid by Electrochemical-Surface Enhanced Raman Spectroscopy Using a Multilayered Au/Ag Substrate. *Anal. Chem.* **2015**, *87*, 441−447.
(31) Zhou, Q.; Meng, G.; Liu, J.; Huang, Z.; Han, F.; Zhu, C.; Kim, D.; Kim, T.; Wu, N. A Hierarchical Nanostructure-Based Surface-Enhanced Raman Scattering Sensor for Preconcentration and Detection of Antibiotic Pollutants. *Adv. Mater. Technol.* **2017**, *2*, No. 1700028.
(32) Li, D.; Li, D.; Fossey, J. S.; Long, Y. Portable Surface-Enhanced Raman Scattering Sensor for Rapid Detection of Aniline and Phenol Derivatives by On-Site Electrostatic Preconcentration. *Anal. Chem.* **2010**, *82*, 9299−9305.
(33) Lynk, T. P.; Sit, C. S.; Brosseau, C. L. Electrochemical Surface-Enhanced Raman Spectroscopy as a Platform for Bacterial Detection and Identification. *Anal. Chem.* **2018**, *90*, 12639−12646.
(34) Gu, H.-Y.; Yu, A.; Chen, H. Direct Electron Transfer and Characterization of Hemoglobin Immobilized on a Au Colloid−Cysteamine-Modified Gold Electrode. *J. Electroanal. Chem.* **2001**, *516*, 119−126.
(35) Kladnik, G.; Puppin, M.; Coreno, M.; de Simone, M.; Floreano, L.; Verdini, A.; Morgante, A.; Cvetko, D.; Cossaro, A. Ultrafast Charge Transfer Pathways Through A Prototype Amino-Carboxylic Molecular Junction. *Nano Lett.* **2016**, *16*, 1955−1959.
(36) He, H.; Li, P.; Tang, X.; Lin, D.; Xie, A.; Shen, Y.; Yang, L. Developing Cysteamine-Modified SERS Substrate for Detection of Acidic Pigment with Weak Surface Affinity. *Spectrochim. Acta, Part A* **2019**, *212*, 293−299.
(37) Simone, G.; van de Donk, O. Short Chain Thiols Induce Better Plasmon Resonance Sensitivity in Au (111). *J. Mater. Chem. C* **2019**, *7*, 13803−13810.
(38) Zhang, J.; Bilič, A.; Reimers, J. R.; Hush, N. S.; Ulstrup, J. Coexistence of Multiple Conformations in Cysteamine Monolayers on Au (111). *J. Phys. Chem. B* **2005**, *109*, 15355−15367.
(39) Wirde, M.; Gelius, U.; Nyholm, L. Self-Assembled Monolayers of Cystamine and Cysteamine on Gold Studied by XPS and Voltammetry. *Langmuir* **1999**, *15*, 6370−6378.
(40) Schmidt, M. S.; Hübner, J.; Boisen, A. Large Area Fabrication of Leaning Silicon Nanopillars for Surface Enhanced Raman Spectroscopy. *Adv. Mater.* **2012**, *24*, OP11−OP18.
(41) Bora, M.; Fasenfest, B. J.; Behymer, E. M.; Chang, A. S.; Nguyen, H. T.; Britten, J. A.; Larson, C. C.; Chan, J. W.; Miles, R. R.; Bond, T. C. Plasmon Resonant Cavities in Vertical Nanowire Arrays. *Nano Lett.* **2010**, *10*, 2832−2837.
(42) Huang, Z.; Meng, G.; Huang, Q.; Yang, Y.; Zhu, C.; Tang, C. Improved SERS Performance from Au Nanopillar Arrays by Abridging the Pillar Tip Spacing by Ag Sputtering. *Adv. Mater.* **2010**, *22*, 4136−4139.
(43) Gartia, M. R.; Xu, Z.; Behymer, E.; Nguyen, H.; Britten, J. A.; Larson, C.; Miles, R.; Bora, M.; Chang, A. S.; Bond, T. C.; Logan Liu, G. Rigorous Surface Enhanced Raman Spectral Characterization of Large-Area High-Uniformity Silver-Coated Tapered Silica Nanopillar Arrays. *Nanotechnology* **2010**, *21*, No. 395701.
(44) Park, J.-W.; Shumaker-Parry, J. S. Structural Study of Citrate Layers on Gold Nanoparticles: Role of Intermolecular Interactions in Stabilizing Nanoparticles. *J. Am. Chem. Soc.* **2014**, *136*, 1907−1921.
(45) Muñoz, P.; Noordam, C. T. N.; Egberink, R. J. M.; Huskens, J.; Garcia-Blanco, S. M. Comparative Study of Multiple Thiol-Based Self-Assembled Monolayer Coatings for the SERS Detection of Nitrite, Nitrate, and Perchlorate Anions in Water. *Appl. Opt.* **2019**, *58*, 9345−9352.
(46) Michota, A.; Kudelski, A.; Bukowska, J. Molecular Structure of Cysteamine Monolayers on Silver and Gold Substrates: Comparative Studies by Surface-Enhanced Raman Scattering. *Surf. Sci.* **2002**, *502*−*503*, 214−218.
(47) Ikeda, K.; Suzuki, S.; Uosaki, K. Enhancement of SERS Background through Charge Transfer Resonances on Single Crystal Gold Surfaces of Various Orientations. *J. Am. Chem. Soc.* **2013**, *135*, 17387−17392.
(48) Wang, L.; Roitberg, A.; Meuse, C.; Gaigalas, A. K. Raman and FTIR Spectroscopies of Fluorescein in Solutions. *Spectrochim. Acta, Part A* **2001**, *57*, 1781−1791.
(49) Gonçalves, M. R.; Enderle, F.; Marti, O. Surface-Enhanced Raman Spectroscopy of Dye and Thiol Molecules Adsorbed on Triangular Silver Nanostructures: A Study of Near-Field Enhancement, Localization of Hot-Spots, and Passivation of Adsorbed Carbonaceous Species. *J. Nanotechnol.* **2012**, *2012*, 1−15.
(50) Hildebrandt, P.; Stockburger, M. Surface Enhanced Resonance Raman Study on Fluorescein Dyes. *J. Raman Spectrosc.* **1986**, *17*, 55−58.
(51) Li, T.; Guo, L.; Wang, Z. Gold Nanoparticle-Based Surface Enhanced Raman Scattering Spectroscopic Assay for the Detection of Protein-Protein Interactions. *Anal. Sci.* **2008**, *24*, 907−910.
(52) Cao, Q.; Che, R.; Chen, N. Facile and Rapid Growth of Ag2S Microrod Arrays as Efficient Substrates for both SERS Detection and Photocatalytic Degradation of Organic Dyes. *Chem. Commun.* **2014**, *50*, 4931−4933.
(53) Shan, F.; Zhang, X.; Fu, X.; Zhang, L.; Su, D.; Wang, S.; Wu, J.; Zhang, T. Investigation of Simultaneously Existed Raman Scattering Enhancement and Inhibiting Fluorescence using Surface Modified Gold Nanostars as SERS Probes. *Sci. Rep.* **2017**, *7*, No. 6813.
(54) Meyer, S. A.; Ru, E. C. L.; Etchegoin, P. G. Quantifying Resonant Raman Cross Sections with SERS. *J. Phys. Chem. A* **2010**, *114*, 5515−5519.
(55) Kim, Y. H.; Kim, K.; D'Argenio, D. Z.; Crandall, E. D. Characteristics of Passive Solute Transport across Primary Rat Alveolar Epithelial Cell Monolayers. *Membranes* **2021**, *11*, No. 331.
(56) Hussain, A.; Pu, H.; Sun, D. SERS Detection of Sodium Thiocyanate and Benzoic Acid Preservatives in Liquid Milk using Cysteamine Functionalized Core-Shelled Nanoparticles. *Spectrochim. Acta, Part A* **2020**, *229*, No. 117994.
(57) Racicot, J. M.; Mako, T. L.; Olivelli, A.; Levine, M. A Paper-Based Device for Ultrasensitive, Colorimetric Phosphate Detection in Seawater. *Sensors* **2020**, *20*, 2766.
(58) Massarini, E.; Wästerby, P.; Landström, L.; Lejon, C.; Beck, O.; Andersson, P. O. Methodologies for Assessment of Limit of Detection and Limit of Identification using Surface-Enhanced Raman Spectroscopy. *Sens. Actuators, B* **2015**, *207*, 437−446.
(59) Wu, K.; Rindzevicius, T.; Schmidt, M. S.; Mogensen, K. B.; Xiao, S.; Boisen, A. Plasmon Resonances of Ag Capped Si Nanopillars Fabricated using Mask-less Lithography. *Opt. Express* **2015**, *23*, 12965−12978.
(60) Chevalier, R. B.; Dwyer, J. R. Optimizing Noncontact Oxygen-Plasma Treatment to Improve the Performance of a Top-Down Nanofabricated Surface Enhanced Raman Spectroscopy Substrate with Structurally Responsive, High-Aspect-Ratio Nanopillar Array. *J. Raman Spectrosc.* **2021**, *52*, 608−615.
(61) Laetsch, T.; Downs, R. Software for Identification and Refinement of Cell Parameters from Powder Diffraction Data of Minerals using the RRUFF Project and American Mineralogist Crystal Structure Databases In *Abstracts from the 19th General Meeting of the International Mineralogical Association*, 2006; pp 23−28.

NOTE ADDED AFTER ASAP PUBLICATION

Due to a production error, this article originally published with unrelated text in Figure 5C. The corrected figure published May 9, 2022.

https://doi.org/10.1021/acsami.2c02934
ACS Appl. Mater. Interfaces XXXX, XXX, XXX−XXX